Received: 23 December 2025 | Revised: 25 March 2026 | Accepted: 20 April 2026

DOI: 10.1002/inmd.70135

RESEARCH ARTICLE

Interdisciplinary MEDICINE

Biomimetic mineralization-inspired formulation-adjuvant integrated circRNA nanovaccine against COVID-19

Liangru Lin[1,2,3,4,5] | **Yingying Ren**[1,4] | **Jing Li**[1,4] | **Panxing Ren**[1,4] | **Xinran Wang**[1,4] | **Yixin Ding**[1,6] | **Linsu Liu**[1,4] | **Cong Liu**[1,4] | **Zhou Li**[3,7] | **Yan Liu**[2] | **Dan Luo**[1,4]

[1]Beijing Institute of Nanoenergy and Nanosystems, Beijing Key Laboratory of High-Entropy Energy Materials and Devices, Chinese Academy of Sciences, Beijing, China

[2]Central Laboratory, Department of Orthodontics, Peking University School and Hospital for Stomatology & National Center for Stomatology & National Clinical Research Center for Oral Diseases & National Engineering Research Center of Oral Biomaterials and Digital Medical Devices & Beijing Key Laboratory of Digital Stomatology & Research Center of Engineering and Technology for Computerized Dentistry Ministry of Health & NMPA Key Laboratory for Dental Materials & National Engineering Research Center of Oral Biomaterials and Digital Medical Devices, Beijing, China

[3]Vita Tech Innovation Center, Beijing Tsinghua Changgung Hospital, School of Clinical Medicine Tsinghua University, Beijing, China

[4]School of Nanoscience and Technology, University of Chinese Academy of Sciences, Beijing, China

[5]Huairou Laboratory, Beijing, China

[6]Department of Cancer Medical Center, Peking Union Medical College Hospital, Chinese Academy of Medical Science & Peking Union Medical College, Beijing, China

[7]School of Biomedical Engineering, Tsinghua Medicine, Tsinghua University, Beijing, China

Correspondence
Cong Liu, Zhou Li, Yan Liu and Dan Luo.
Email: liucong@binn.cas.cn, li_zhou@tsinghua.edu.cn, orthoyan@bjmu.edu.cn and luodan@binn.cas.cn

Funding information
National Natural Science Foundation of China, Grant/Award Numbers: 52372174, 82230030, T2125003; National Key Research and Development Program of China, Grant/Award Number: 2022YFB3205602; Beijing Nova Programme Interdisciplinary Cooperation Project, Grant/Award Number: 20250484970

Abstract

Conventional RNA-based vaccines rely on lipid nanoparticles (LNPs) for delivery; however, concerns exist regarding the potential systemic toxicity of their chemical composition, and their immune-activating capabilities require further enhancement. Inspired by Mg^{2+} as a key ion for maintaining RNA secondary structure stability, we developed a one-pot method for directly synthesizing a circular RNA-based formulation-adjuvant integrated nanovaccine (CircRNA@FAiNVac) capable of delivering programmed circular RNA (circRNA) based on biomimetic mineralization principles. Specifically, during circRNA rolling circle transcription, the controllable crystallization of magnesium pyrophosphate (MgPPi) nanoparticles was achieved by enhancing the reaction kinetics between ribonucleotide triphosphates and Mg^{2+}, thereby encapsulating circRNA within the nanoparticles and forming a protective carrier that also functions as an adjuvant. Based on the specific hydrolysis of MgPPi by pyrophosphatase, CircRNA@FAiNVac can efficiently release RNA intracellularly, thereby facilitating gene expression. Unlike LNPs, which often

Liangru Lin, Yingying Ren and Jing Li contributed equally.

contain toxic excipients, the vector structure of CircRNA@FAiNVac consisted only of nucleic acid precursors and ions, exhibiting good biocompatibility and reducing adverse reactions. More importantly, CircRNA@FAiNVac possessed potent immune activation capabilities; its self-adjuvanting activity promoted multimodal immune activation, enhancing both humoral and cellular responses. Animal experiments confirmed that the innovative design of CircRNA@FAiNVac ensured stable and sustained autonomous expression of the SARS-CoV-2 receptor-binding domain, while the nanostructure activated multiple immune pathways, providing potent protection. The formulation-adjuvant integration strategy of CircRNA@FAiNVac based on biomimetic mineralization principles provides an alternative approach for the development of next-generation vaccines. Based on antigen sequence optimization, it enables rapid customized development of vaccines targeting variant strains.

KEYWORDS
biomimetic mineralization, circRNA, nanovaccine, self-adjuvant, self-assembly

1 | INTRODUCTION

Coronavirus Disease 2019 (COVID-19), caused by severe acute respiratory syndrome coronavirus 2 (SARS-CoV-2), remains a significant public health challenge, with over 775 million confirmed cases and 15 million deaths worldwide.[1,2] While mRNA vaccines have been pivotal in combating the pandemic, their limitations are increasingly apparent.[3–6] Inherent instability necessitates extensive chemical modifications (e.g., 1-methylpseudouridine) and a stringent cold chain, hindering deployment in resource-limited regions.[7–11] In contrast, circular RNA (circRNA) offers a structurally superior alternative.[12,13] Its covalently closed, continuous loop conformation confers exceptional resistance to exonuclease degradation, extending its intracellular half-life several-fold compared to linear mRNA and reducing the need for nucleoside modification.[12,14] When engineered with elements such as internal ribosome entry sites, circRNA enables robust and sustained protein expression, demonstrating significant promise as a next-generation vaccine platform.[12,15] Preclinical studies have demonstrated that circRNA vaccines can elicit potent and durable immune responses against SARS-CoV-2 variants, highlighting their superior potential for durable immunization.[12] Nevertheless, the efficacy of any nucleic acid therapeutic, including circRNA, is critically contingent upon a safe and effective delivery vehicle capable of protecting the cargo and facilitating its intracellular release.[5,16]

The current paradigm for mRNA delivery primarily relies on lipid nanoparticles (LNPs).[17–19] While clinically validated, LNP technology faces pressing challenges beyond the stabilization of its nucleic acid.[20–22] First, the synthetic components of LNPs, including ionizable lipids and polyethylene glycol (PEG) ylated lipids, raise non-negligible concerns regarding potential systemic toxicity, immunogenicity, and long-term biodistribution profiles.[23,24] Furthermore, certain functional excipients, such as specific oxysterols (e.g., 20α/20β-hydroxycholesterol) that are incorporated to modulate membrane fluidity, may paradoxically enhance phagocytic clearance and lysosomal degradation, thereby reducing the intended protein expression.[25–27] Most critically, the immunostimulatory properties of LNPs can be suboptimal or unpredictable; attempting to increase potency or redirect biodistribution beyond the liver often necessitates higher doses, which in turn can exacerbate inflammatory side effects and immune-related toxicity.[28,29] Hence, these challenges underscore an urgent need for novel delivery platforms that are inherently biocompatible, simpler to manufacture, and capable of potent and programmable immunostimulation.[30–34]

Here, we report a revolutionary delivery platform inspired by biomimetic mineralization. We developed a facile one-pot method to directly synthesize a circRNA-based formulation-adjuvant integrated nanovaccine (CircRNA@FAiNVac) capable of delivering programmed circRNA (Figure 1). Our innovative strategy leverages the dual biological roles of magnesium ions (Mg^{2+}): as essential cofactors for polymerase activity and RNA structural integrity, and as inorganic precursors for carrier synthesis. Specifically, during the rolling circle

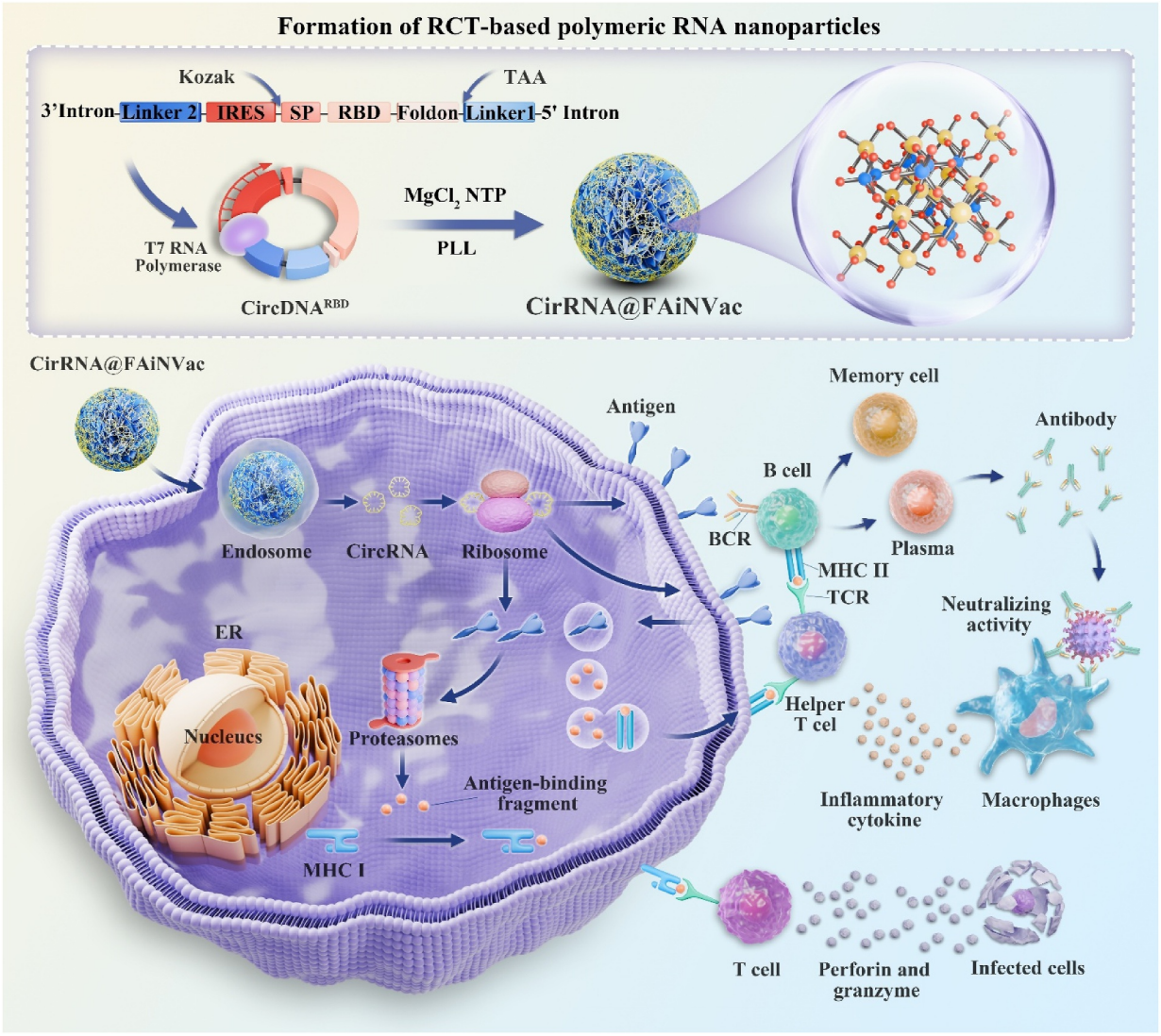

FIGURE 1 Schematic diagram of engineered RNA nanopaticles (CircRNA@FAiNVac) as a safe and self-adjuvanting platform for COVID-19 vaccination. The synthesis of formulation-adjuvant integrated nanovaccine (CircRNA@FAiNVac) is achieved by a one-pot method based on biomimetic mineralization principles, by which MgPPi directly encapsulates circRNA into nanoparticles as a protective carrier and simultaneously as an adjuvant. Notably, self-adjuvanting property endows potent immunostimulatory activity to CircRNA@FAiNVac via facilitating multimodal immune activation: antigen peptides presented via MHC I activated cytotoxic T cells, inducing a cellular immune response, while those presented via MHC II activated helper T cells, which in turn activated B cells to produce antibodies, thereby achieving humoral immunity.

transcription (RCT) of circRNA, we precisely controlled the reaction kinetics to drive the controllable crystallization of magnesium pyrophosphate (MgPPi) nanoparticles. This process seamlessly entrapped the nascent circRNA within the growing inorganic matrix, yielding a protective inorganic carrier that inherently functions as an adjuvant. This CircRNA@FAiNVac platform is fundamentally distinct in composition, consisting solely of natural biochemical precursors (ribonucleotide triphosphates) and physiological ions, thereby exhibiting superior biocompatibility and minimizing excipient-related risks. More importantly, as a formulation-adjuvant integrated nanovaccine, CircRNA@FAiNVac exhibited strong immune activation capabilities, promoting multimodal innate immune activation that significantly enhances both humoral and cellular adaptive responses. As confirmed in animal studies, this innovative design ensured stable and sustained in vivo antigen expression while concurrently activating multiple protective immune pathways. Collectively, this

CircRNA@FAiNVac platform, based on a biomimetic mineralization and formulation-adjuvant integrated strategy, provides a versatile and promising alternative for next-generation vaccine development.

2 | RESULTS AND DISCUSSION

2.1 | Preparation and characterization of CircRNA@FAiNVac

The CircRNA@FAiNVac platform was constructed through a one-pot biomimetic mineralization strategy. The process begins with the modular encoding of the SARS-CoV-2 receptor-binding domain (RBD) antigen sequence onto a linear DNA template, which is subsequently circularized to serve as the template for RCT. Utilizing T7 RNA polymerase, long tandem repeats of circRNA were synthesized. Crucially, by enhancing the reaction kinetics between ribonucleotide triphosphates and Mg^{2+} ions, we achieved controllable crystallization of MgPPi nanoparticles during the RCT process. A Mg^{2+}: rNTP molar ratio of 6:1 precisely balances the Mg^{2+} requirement for RCT catalysis and the supersaturation threshold required for controlled MgPPi crystallization (Figure S1 and Table S1). Encapsulation efficiency (EE%) significantly increased with increasing Mg^{2+} concentration until reaching a peak at the Mg^{2+}: rNTP molar ratio of 6:1, after which EE% began to decrease (Table S1). This biomimetic mineralization step simultaneously encapsulated the synthesized circRNA within the forming MgPPi crystals, resulting in a core-shell nanostructure that functions as both a protective carrier and an intrinsic immune adjuvant (Figure 2A). To promote efficient in vivo delivery, the initially formed nanoparticles were modified with poly-L-lysine (PLL) via molecular electrostatic forces to form nanoscale formulations.[35] The resulting nanoparticles exhibited a uniform dispersion in aqueous solution as evidenced by the distinct Tyndall effect (Figure 2B). As a comparison, CircRNA^{EV}@FAiNVac is an RNA nanoparticle constructed with a DNA template of circular RNA that does not contain the RBD sequence. Transmission electron microscopy (TEM) and scanning electron microscopy (SEM) revealed that the final CircRNA@FAiNVac nanoparticles were monodisperse with a spherical morphology (Figure 2C,D). High-resolution TEM imaging confirmed that CircRNA@FAiNVac showed a clear crystal structure with a lattice size of approximately 0.35 nm, corresponding to the (022) crystal plane of monoclinic MgPPi (Figure 2E). Dynamic light scattering (DLS) analysis corroborated the nanoscale size showing an average hydrodynamic diameter of about 43 nm (Figure 2F). The surface modification of PLL converted the originally negatively charged CircRNA@FAiNVac into positively charged (Figure 2G). The composition of CircRNA@FAiNVac was analyzed using scanning TEM (STEM)-based energy dispersive X-ray spectroscopy (EDS) analysis, and the results showed that all particles were mainly composed of C, N, O, Mg, and P (Figure 2H and Figure S2). The presence of C and N in the particles indicated the presence of RNA in CircRNA@FAiNVac, while the presence of Mg, P, and O indicated the structure of MgPPi. Further EDS mapping and RNA loading quantitative analysis addressed the concern regarding the possible formation of magnesium-phosphoprotein nanoparticles lacking RNA or "empty shell" structures. Through complementary characterization methods, the distribution of circRNA within the mineralized nanoparticles was verified. Specifically, the EDS mapping results clearly showed that the elemental distribution of N (from circRNA), P (from MgPPi and circRNA) and Mg (from MgPPi) was uniform throughout the nanoparticle structure (Figure 2H). This uniform elemental distribution confirmed that the circRNA was closely embedded within the mineralized nanoparticles rather than forming independent "empty shell" particle groups lacking RNA. Additionally, the RNA loading analysis revealed that the formed nanoparticles still retained a significant amount of circRNA content (Table S1). In summary, the results of EDS mapping and RNA loading analysis clearly confirmed the absence of significant "empty" magnesium phosphate ester nanoparticles, thereby verifying the structural and functional integrity of the CircRNA@FAiNVac formulation. Controllable crystallization of MgPPi nanoparticles was achieved by fine-tuning the reaction kinetics, including the molar ratio of ribonucleotide triphosphates and Mg^{2+}, reaction temperature, and incubation time. These parameters collectively regulated the nucleation and growth of MgPPi crystals, ensuring the formation of uniform nanoparticles with appropriate size and efficient circRNA encapsulation. Furthermore, the uniform distribution of the elements indicated that the polymerized circRNA was uniformly loaded into CircRNA@FAiNVac. Gel electrophoresis analysis showed that all CircRNA@FAiNVac samples presented smear bands in agarose gel, indicating that the synthesized nucleic acid molecules have a length of over 5000 bp (Figure 2I). Ultraviolet-visible spectroscopy (UV-vis) spectroscopy and circular dichroism (CD) spectroscopy jointly confirmed the effective loading of nucleic acids on CircRNA@FAiNVac and suggested the preservation of RNA secondary and tertiary

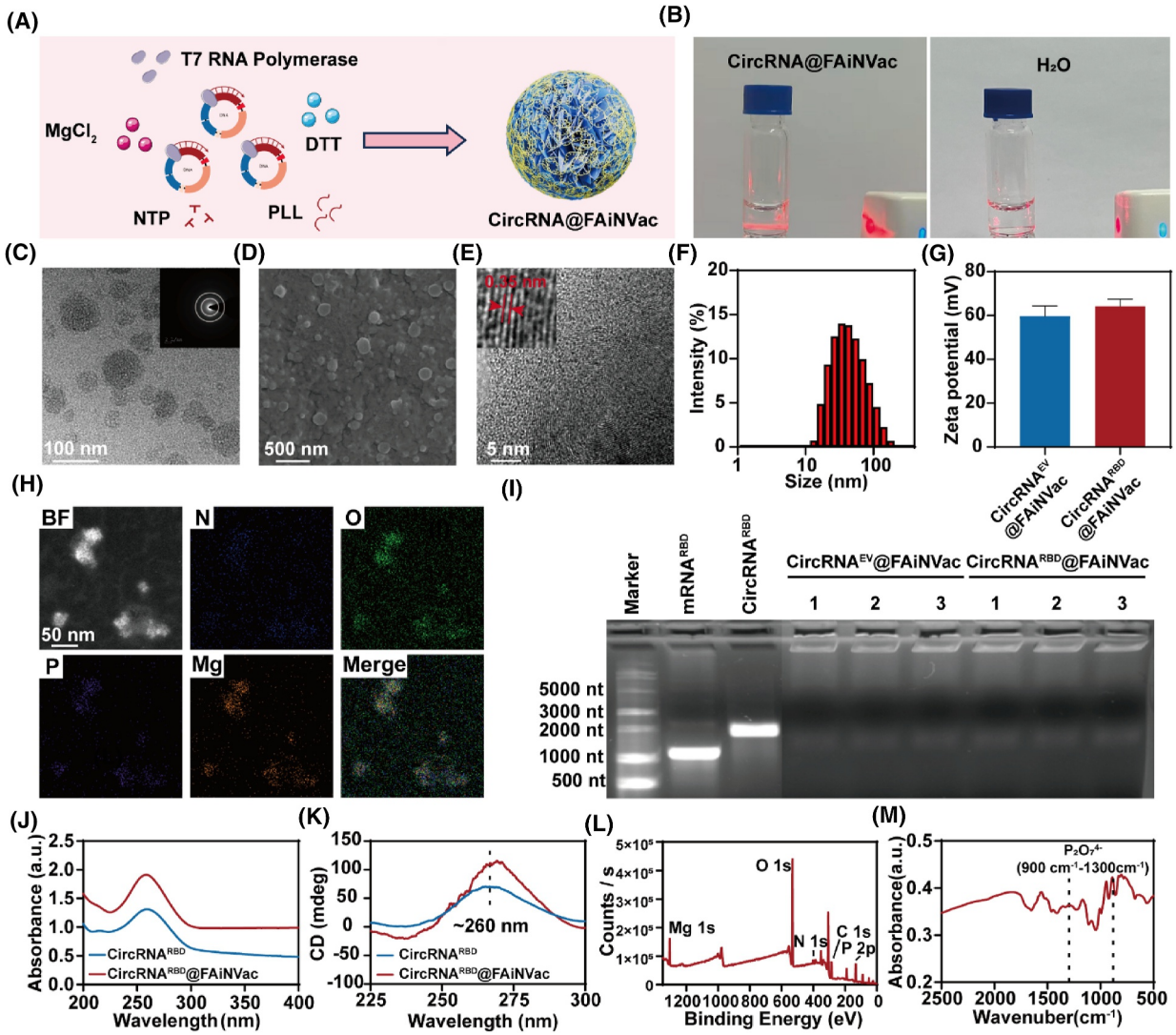

FIGURE 2 Physicochemical characterization of CircRNA@FAiNVac. (A) Schematic diagram of the CircRNA@FAiNVac synthesized from circular DNA. (B) CircRNA@FAiNVac exhibits a distinct Tyndall effect compared to Water. (C) Transmission electron microscopy (TEM) image of CircRNA@FAiNVac. (D) SEM image of CircRNA@FAiNVac. (E) Lattice imaging analysis of CircRNA@FAiNVac. (F) Particle size of CircRNA@FAiNVac. (G) Zeta potential of CircRNA@FAiNVac. Data are shown as the mean ± SEM ($n = 3$). (H) STEM-based energy dispersive spectroscopy (EDS) mapping of CircRNA^{RBD}@FAiNVac. (I) Gel electrophoresis image of mRNA^{RBD}, circRNA^{RBD}, CircRNA^{EV}@FAiNVac, and CircRNA^{RBD}@FAiNVac (1-3 indicate the three replicate samples of this group). (J) UV-vis spectra of circRNA^{RBD} and CircRNA^{RBD}@FAiNVac. (K) CD spectra of circRNA^{RBD} and CircRNA^{RBD}@FAiNVac. (L) X-ray photoelectron spectroscopy (XPS) analysis of CircRNA@FAiNVac. (M) FITR of CircRNA@FAiNVac.

structures within the composite (Figure 2J,K). The CircRNA@FAiNVac sample was further characterized by X-ray photoelectron spectroscopy (Figure 2L), which revealed distinct chemical states of corresponding elements, consistent with the results of STEM-based EDS analysis. The higher binding energy (BE) of the Mg 1s peak at 1304.99 eV was assigned to Mg (II) in magnesium pyrophosphate (Figure S3A). Similarly, the higher BE of the P 2p peak at 133.4 eV corresponded to P(V) in magnesium pyrophosphate (Figure S3B). The higher BE of the O 1s peak at 531.23 eV was attributed to O(II) in both magnesium pyrophosphate and RNA (Figure S3C). Moreover, Fourier Transform infrared (FTIR) spectroscopy also uncovered the absorption peaks of phosphate groups of magnesium pyrophosphate (Figure 2M). Collectively, we successfully synthesized MgPPi mineralization-integrated circRNA nanoformulation through the RCT reaction system.

2.2 | In vitro evaluation of CircRNA@FAiNVac as a potential vaccine platform

CircRNA@FAiNVac is capable of achieving stable and sustained expression of the target protein, which is consistent with the structural stability of circRNAs (Figure S4). To verify the protein expression capability of the CircRNA@FAiNVac platform, we first synthesized CircRNA@FAiNVac encoding the enhanced green fluorescent protein sequence and delivered it to HEK293T cells (Figure 3A). Through fluorescence microscopy, obvious green fluorescent protein expression could be detected (Figure 3B), and quantitatively confirmed by flow cytometry, which showed a significantly higher fluorescence intensity compared to control groups (Figure 3C). To evaluate the application potential of this platform in antigen expression, we further detected the RBD antigen concentration in the supernatant to be approximately 136 ng/mL, which was significantly higher than that of control groups (Figure 3D). At the same time, effective expression was observed at both 12 and 24 h (Figure 3E,F), demonstrating that CircRNA@FAiNVac enables sustained and high-level antigen production, which is a critical feature for vaccine efficacy. Notably, this positive uptake and expression result in non-immune, non-antigen-presenting HEK-293T cells suggests that the protein expression mediated by CircRNA@FAiNVac is not strictly restricted to professional antigen-presenting cells (APCs), reflecting the broad and efficient delivery adaptability of the MgPPi-based bionic mineralized vector. Safety is a paramount concern for vaccine formulations. The translation efficiency was compared under the same conditions of circular RNA dosage and intracellular delivery. To confirm antigen expression in the key target cells, we evaluated RBD translation in primary bone marrow-derived dendritic cells (BMDCs). Immunofluorescence staining revealed a strong cytoplasmic RBD signal in BMDCs treated with CircRNA@FAiNVac (Figures S5A and S5B). Flow cytometric analysis of intracellular RBD further quantified that over 8.08-fold of BMDCs were antigen-positive following treatment (Figure S5C). For comparison, circRNA was also formulated using a clinically validated LNP platform (DLin-MC3-DMA/DSPC/Cholesterol/DMG-PEG 2000, 50:10:38.5:1.5), which served as the gold standard control for RNA vaccine delivery. Cytotoxicity assessment in HEK293T cells indicated that CircRNA@FAiNVac exhibited significantly lower cytotoxicity compared to conventional LNP-encapsulated circRNA (Figure 3G). More importantly, the innate immune response triggered by CircRNA@FAiNVac was significantly weaker than that of the naked RNA transfection group and the LNP control group in HEK293T cells (Figure 3H–L). This phenomenon may be attributed to the fact that nanoparticles enter cells through endocytosis, partially bypassing the immune recognition pathways—such as TLR3 in the endosome/lysosome, which requires viral RNA binding to be activated.[27] In contrast, naked RNA transfection may directly activate the RIG-I-like receptor pathway in the cytoplasm, triggering a stronger type I interferon response.[36] The CircRNA@FAiNVac platform exhibits a unique dual mechanism of innate immune regulation, achieved through spatial-temporal separation. The MgPPi mineral shell physically shields the encapsulated circRNA from endosomal TLR3 recognition during cellular entry, thereby preventing premature RNA degradation and excessive TLR3-mediated IFN responses. In contrast, the robust adjuvant effect (NF-κB activation and TNF-α secretion) is mediated by the nanoparticle scaffold itself. Following endosomal escape and cytosolic hydrolysis, the released pyrophosphate (PPi) and Mg^{2+} ions activate the cytosolic STING pathway and NLRP3 inflammasome, respectively.[37–42] This design decouples antigen protection from adjuvant activation, resulting in both high antigen expression and potent DC maturation. A potential limitation of this study is the use of a clinically relevant but non-immuno-optimized LNP (DLin-MC3-DMA based) as the control comparator. Recent advances in next-generation LNPs (e.g., immuno-modified LNPs, lipid-polymer hybrids) have demonstrated enhanced immunostimulatory properties. While our MC3-LNP control serves as a rigorous benchmark for clinical translation, future studies directly comparing CircRNA@FAiNVac with these cutting-edge LNP variants are warranted to further elucidate the relative strengths of our platform. Beyond merely serving as a delivery vehicle, CircRNA@FAiNVac demonstrated self-adjuvanting properties essential for vaccine potency. Following delivery of the RBD-encoding CircRNA@FAiNVac into DCs (Figure 3M), it significantly increased the expression level of MHC II molecules (Figure 3N) and enhanced the expression of the co-stimulatory markers CD80 and CD86 (Figure 3O), indicating DC maturation. This feature is beneficial for enhancing the efficiency of the immune response induced by the vaccine. Additionally, the maturation status of DCs was further verified through confocal microscopy (Figure 3P,Q). The self-adjuvanting activity of CircRNA@FAiNVac arises from a hierarchical, synergistic mechanism rather than a single molecular trigger. Analysis of comparative groups revealed that the MgPPi mineral scaffold is the primary initiator of innate immunity, capable of activating NF-κB and MAPK pathways

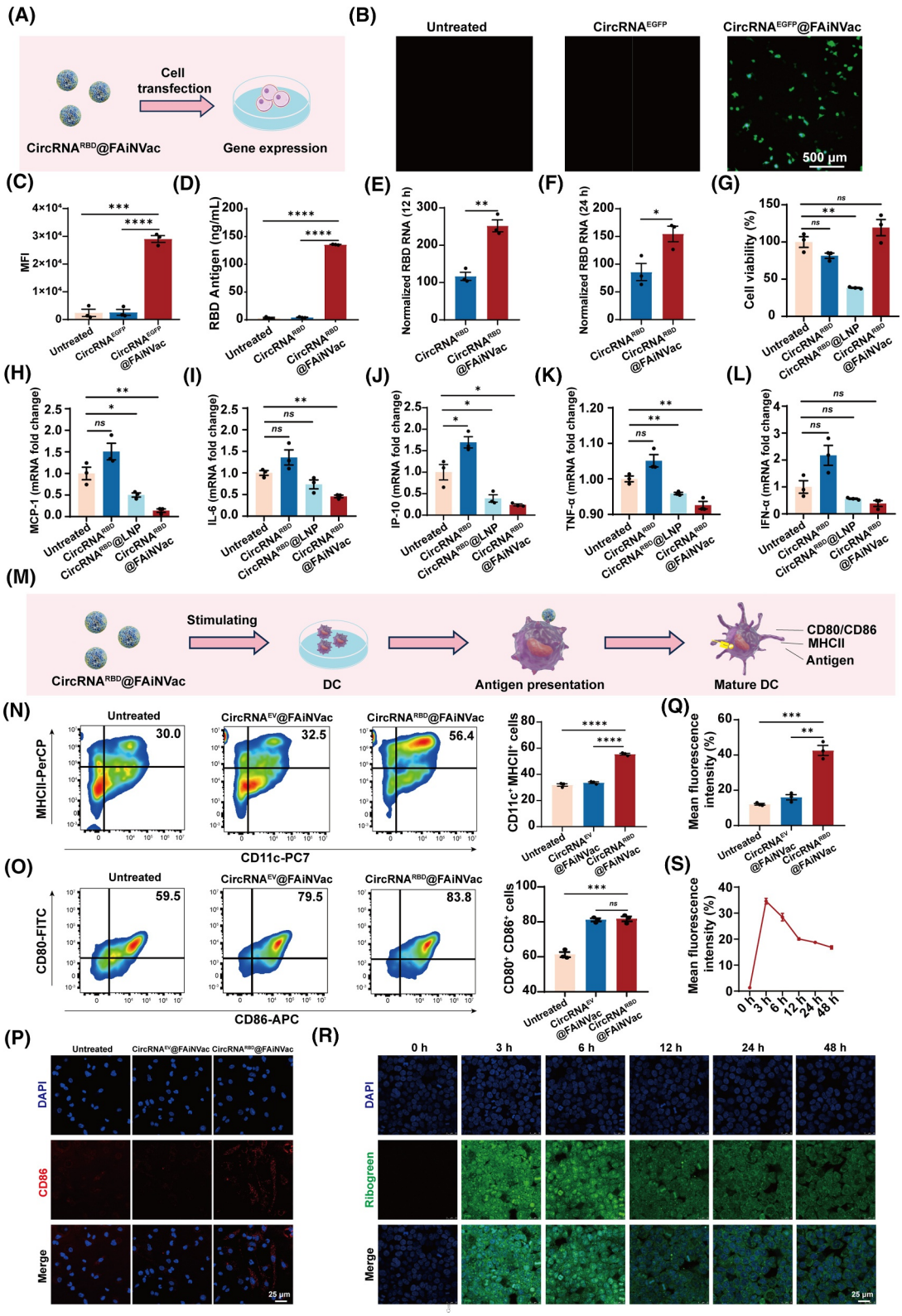

FIGURE 3 Legend on next page.

independently via the release of PPi (STING activator) and Mg^{2+} (NLRP3 activator) (Figure S6). The circRNA cargo, while not a potent innate agonist on its own, provides sustained antigen translation that amplifies this initial signal. This unique integration of innate adjuvantation (by MgPPi) and antigenic persistence (by circRNA) eliminates the need for exogenous adjuvants and drives the robust multimodal immune response observed in this study. In

cellular uptake experiments, nucleic acid-stained CircRNA@FAiNVac was observed to enter the cytoplasm within 3 h and remained effectively internalized over 48 h, with peak uptake occurring at 3 h (Figure 3R,S). Following clathrin-mediated endocytosis, CircRNA@FAiNVac traffics to early endosomes, which subsequently mature into acidic late endosomes/lysosomes (pH 4.5–5.5). The acidic microenvironment triggers the partial dissolution of MgPPi nanoparticles, a process that sequesters protons and induces osmotic swelling (proton sponge effect). This leads to the rupture of the endosomal membrane and the release of the nanoparticle core into the cytoplasm, as confirmed by confocal microscopy showing dissociation from LysoTracker staining at 1 and 3 h post-internalization (Figure S7). Upon reaching the cytosol, the residual MgPPi matrix is rapidly hydrolyzed by endogenous cytosolic pyrophosphatase (PPA). This dual-step release mechanism—initial endosomal escape via pH-responsive dissolution followed by cytosolic hydrolysis—ensures the efficient liberation of functional circRNA for translation. Overall, the CircRNA@FAiNVac platform exhibits notable advantages in antigen expression, safety, and immune activation, demonstrating broad potential for vaccine development.

2.3 | Transcriptomics analysis reveals CircRNA^{RBD}@FAiNVac-induced dendritic cell maturation mechanisms

To elucidate the molecular mechanisms underlying the immunostimulatory activity of CircRNA^{RBD}@FAiNVac as a vaccine, we conducted transcriptome-wide RNA sequencing (RNA-seq) analysis on DCs that were either untreated, treated with CircRNA^{EV}@FAiNVac, or treated with CircRNA^{RBD}@FAiNVac. The results of clustering analysis revealed that compared with the CircRNA^{EV}@FAiNVac or untreated groups, DCs treated with CircRNA^{RBD}@FAiNVac exhibited upregulation of genes associated with inflammatory immune response (Figure 4A and Figure S8). Pathway enrichment analysis further demonstrated that cells in the CircRNA^{RBD}@FAiNVac group displayed enhanced immune and defense responses, with significant enrichment of multiple inflammation-related pathways, including TNF signaling, NF-κB signaling, and MAPK cascade signaling, as well as DC maturation-related pathways (Figure 4B,C and Figures S9 and S10). The results of differential gene expression analysis revealed that compared with the CircRNA^{EV}@FAiNVac or untreated groups, DCs treated with CircRNA^{RBD}@FAiNVac exhibited upregulation of genes associated with proliferation, differentiation, migration, and maturation abilities, antigen presentation capacity, chemokine and cytokine production, antiviral function, and a series of activating immune response (Figure 4D–G and Figures S11 and S12). Collectively, these findings indicate that CircRNA^{RBD}@FAiNVac has the potential to induce DC pro-inflammatory maturation, thereby providing a theoretical foundation for its application as a vaccine.

Upon CircRNA^{RBD}@FAiNVac treatment, the circRNA component of CircRNA^{RBD}@FAiNVac enters DCs via endocytosis and is subsequently released from the endosome. Under the guidance of ribosomes, the circRNA is translated into antigen proteins. These antigen proteins are

FIGURE 3 In Vitro validation of CircRNA@FAiNVac as a vaccine adjuvant platform. (A) Schematic diagram of CircRNA@FAiNVac transfection into HEK293T cells. (B) Fluorescence microscope image of enhanced green fluorescent protein (EGFP) expression in HEK293T cells transfected with CircRNA^{EGFP}@FAiNVac. (C) Flow cytometry statistics of EGFP expression in HEK293T cells transfected with CircRNA^{EGFP}@FAiNVac. (D) ELISA detection of receptor-binding domain (RBD) protein expression in HEK293T cells transfected with CircRNA^{RBD}@FAiNVac. (E, F) The mRNA abundance of RBD induced by circRNA^{RBD} and CircRNA^{RBD}@FAiNVac via RT-qPCR analysis in HEK293T cells. The mRNA levels were normalized by *GAPDH*. The mRNA fold changes were normalized using the untreated HEK293T cells. (G) Cell viability of HEK293T cells transfected with circRNA^{RBD}, CircRNA^{RBD}@LNP, and CircRNA^{RBD}@FAiNVac for 24 h. (H-L) The mRNA abundance of cytokines MCP-1 (H), IL-6 (I), IP-10 (J), TNF-α (K), and IFN-α (L) induced by circRNA^{RBD}, CircRNA^{RBD}@LNP, and CircRNA^{RBD}@FAiNVac via RT-qPCR analysis in HEK293T cells. The mRNA levels were normalized by *GAPDH*. (M) Schematic illustration of innate immune activation in dendritic cell (DC) cells following CircRNA^{RBD}@FAiNVac transfection. (N) Flow cytometry analysis of MHCII after CircRNA^{EV}@FAiNVac and CircRNA^{RBD}@FAiNVac transfection into DC cells, raw data on the left and statistics on the right. (O) Flow cytometry analysis of CD80 and CD86 after CircRNA^{EV}@FAiNVac and CircRNA^{RBD}@FAiNVac transfection into DC cells, raw data on the left and statistics on the right. (P) Confocal microscopy images of CD86 and DAPI staining. (Q) Statistical analysis of CD86 Fluorescence Values under Confocal Microscopy. (R) Time-dependent uptake of CircRNA@FAiNVac by HEK293T cells, visualized via DAPI staining of nuclei and Ribogreen staining of circRNA in confocal microscopy images. (S) Statistical analysis of the changes in the uptake of CircRNA@FAiNVac by HEK293T cells over time under confocal microscopy. The data are shown as SEM ± mean ($n = 3$). Unpaired two-sided Student *t*-tests were conducted for comparison, as shown in the figure, *$p < 0.05$; **$p < 0.01$; ***$p < 0.001$; ****$p < 0.0001$; ns, not significant. Each symbol represents a separate mouse.

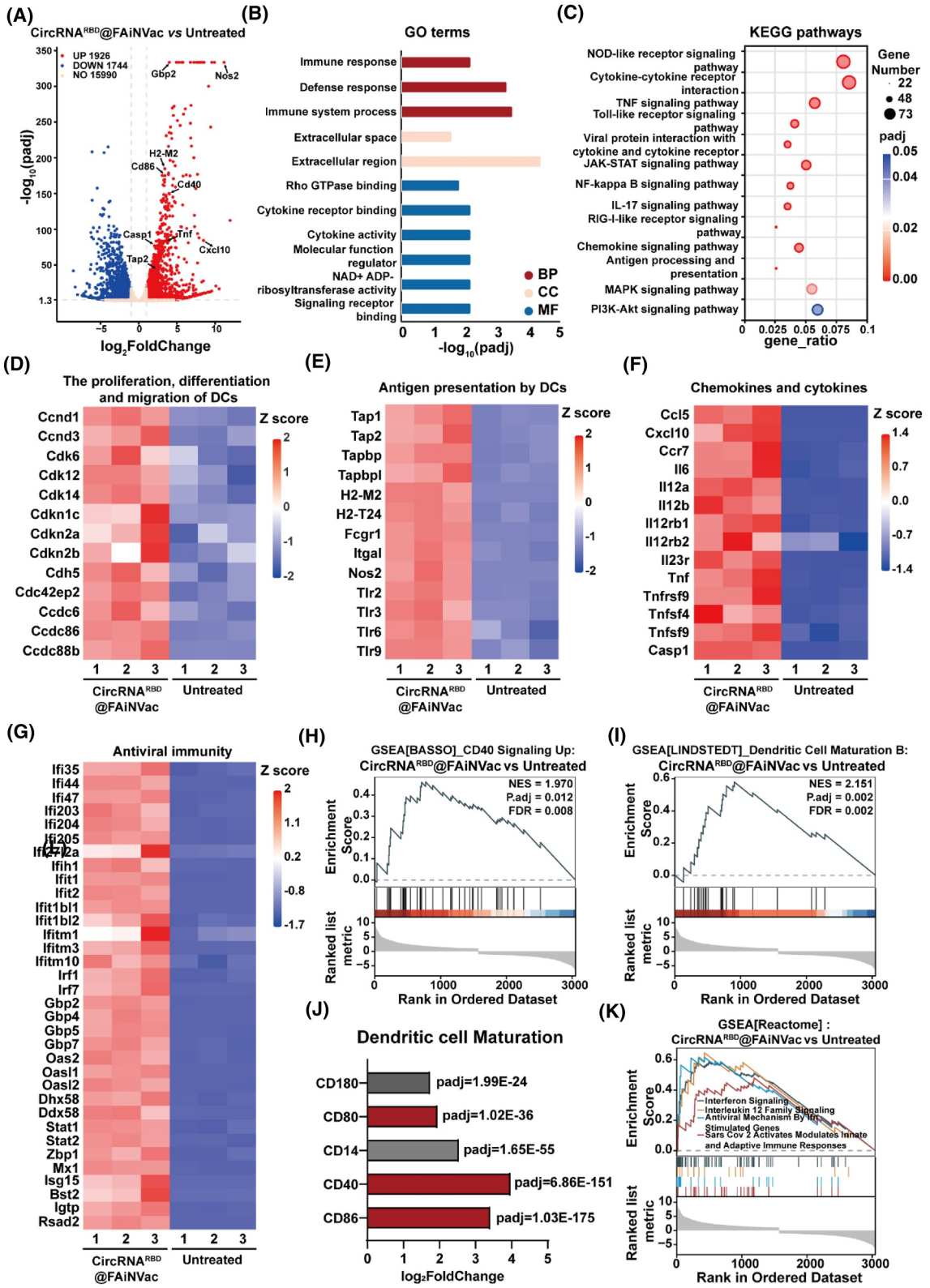

FIGURE 4 Legend on next page.

then degraded by the proteasome into antigen peptides, which bind to MHC I molecules synthesized in the endoplasmic reticulum and are presented on the cell surface. Concurrently, DC activation led to marked upregulation of the CD40 signaling pathway (Figure 4H and Figure S13). This enhanced CD40 signaling promotes cell survival and inflammatory factor secretion through the activation of MAPK and NF-κB pathways, while also synergistically

inducing the co-expression of co-stimulatory molecules CD80 and CD86, ultimately driving DC maturation (Figure 4I,J, Figures S14 and S15).

Notably, compared with CircRNA^{EV}@FAiNVac, CircRNA^{RBD}@FAiNVac showed significant enrichment in calcium ion transmembrane transport and nucleic acid binding-related pathways, further validating the molecular mechanism by which CircRNA^{RBD}@FAiNVac utilizes circRNA expression to induce DC maturation through antigen presentation (Figure S14). It is particularly noteworthy that pathways related to the activation and regulation of innate and adaptive immune responses by SARS-CoV-2 were significantly enriched in the CircRNA^{RBD}@FAiNVac group compared to the PBS or CircRNA^{EV}@FAiNVac groups (Figure 4K and Figure S16). This observation suggests that CircRNA^{RBD}@FAiNVac effectively presents the RBD antigen on DCs, which is crucial for the subsequent generation of antibodies against SARS-CoV-2. In conclusion, these results demonstrate that CircRNA^{RBD}@FAiNVac can significantly enhance the immune response of DCs, driving them toward an inflammatory mature state and optimizing antigen presentation capabilities by activating key inflammatory and co-stimulatory pathways. This mechanism underpins the antiviral effect of CircRNA^{RBD}@FAiNVac as a vaccine candidate.

2.4 | CircRNA@FAiNVac nanovaccine elicits robust RBD-specific antibodies and immune responses

The data in Figure S17 presents the measured results of the temporal variation of fluorescent enzyme protein in BALB/c mice. To evaluate the in vivo immunogenicity and protective potential of the CircRNA@FAiNVac platform, we immunized BALB/c mice via intramuscular injection with 10 μg of the vaccine in a prime-boost regimen at a 2-week interval (Figure 5A). Then, 2 weeks after the boost dose, the sera from immunized mice were collected to detect RBD-Delta-specific antibodies (Figure 5A). Sample sizes were chosen based on preliminary experimental data and established practices for early proof-of-concept studies in the vaccine and nanomedicine fields.[43,44] The vaccine elicited a robust humoral immune response. Serum analysis revealed that CircRNA^{RBD}@FAiNVac triggered a high level of RBD-specific IgG endpoint geometric mean titer, reaching ~4.3 × 10^4 (Figure 5B). Further, we investigated the balance of Th1/Th2 immune responses of the CircRNA^{RBD}@FAiNVac. ELISA showed that CircRNA^{RBD}@FAiNVac triggered IgG1 (Figure 5C) and IgG2a (Figure 5D) at relatively high levels. The ratio of IgG2a/IgG1 was also higher compared to the control group (Figure 5E), indicating a Th1-skewed response. This bias is advantageous for SARS-CoV-2 clearance and helps mitigate the risk of vaccine-associated enhanced respiratory disease, which is often associated with a Th2-dominant profile.[12] More importantly, the results of the pseudovirus neutralization test (Figure S18) showed that the serum of mice vaccinated with CircRNA@FAiNVac exhibited strong antiviral neutralizing activity in vitro, with a high value of the median effective concentration (NT50) of the neutralizing antibodies. These neutralizing antibodies were able to effectively prevent the invasion of the SARS-CoV-2 pseudovirus into host cells, which directly confirmed that the antigen-specific antibodies induced by the vaccine are functional protective antibodies rather than merely binding antibodies. These combined results demonstrate that CircRNA@FAiNVac not only stimulates strong antigen-specific antibody production but also induces high-titer functional neutralizing antibodies, laying a solid foundation for effective antiviral protection in vivo.

FIGURE 4 Transcriptomics analysis reveals CircRNA^{RBD}@FAiNVac -induced dendritic cell (DC) maturation mechanisms. (A) The volcano plot shows the comparison of differentially expressed genes between the CircRNA^{RBD}@FAiNVac groups and the untreated group in DC. Antigen presentation process: Nos2, H2-M2, Tap2; Antiviral immune process: Gbp2; DC maturation markers: CD86, CD40; Cytokines and chemokines: TNF, Cxcl10, Casp1. (B) GO analysis reveals upregulated pathways in CircRNA^{RBD}@FAiNVac versus Untreated DCs (n = 3). (C) KEGG analysis of upregulated pathways in CircRNA^{RBD}@FAiNVac versus Untreated Groups (n = 3). (D) Heatmap depicting differential expression of proliferation/differentiation/migration-related genes in DCs: CircRNA^{RBD}@FAiNVac versus Untreated groups (n = 3). (E) Heatmap revealing differential expression patterns of antigen presentation-related genes in DCs: CircRNA^{RBD}@FAiNVac versus Untreated comparison (n = 3). (F) Heatmap illustration of differential chemokine/cytokine gene expression in DCs: CircRNA^{RBD}@FAiNVac versus Untreated groups (n = 3). (G) Heatmap revealing differential expression of antiviral immune-related genes in DCs: CircRNA^{RBD}@FAiNVac versus Untreated groups (n = 3). (H) GSEA identifies enhanced CD40 signaling up in CircRNA^{RBD}@FAiNVac versus Untreated DCs (n = 3). (I) GSEA reveals enriched DC maturation pathways in CircRNA^{RBD}@FAiNVac versus Untreated DCs (n = 3). (J) Differential expression of DC maturation markers in CircRNA^{RBD}@FAiNVac versus Untreated groups (n = 3). (K) GSEA identifies enriched pathways in DCs: Interferon Signaling, IL-12 family signaling, antiviral mechanisms, and SARS-CoV-2-activated immune responses (CircRNA^{RBD}@FAiNVac vs. Untreated, n = 3).

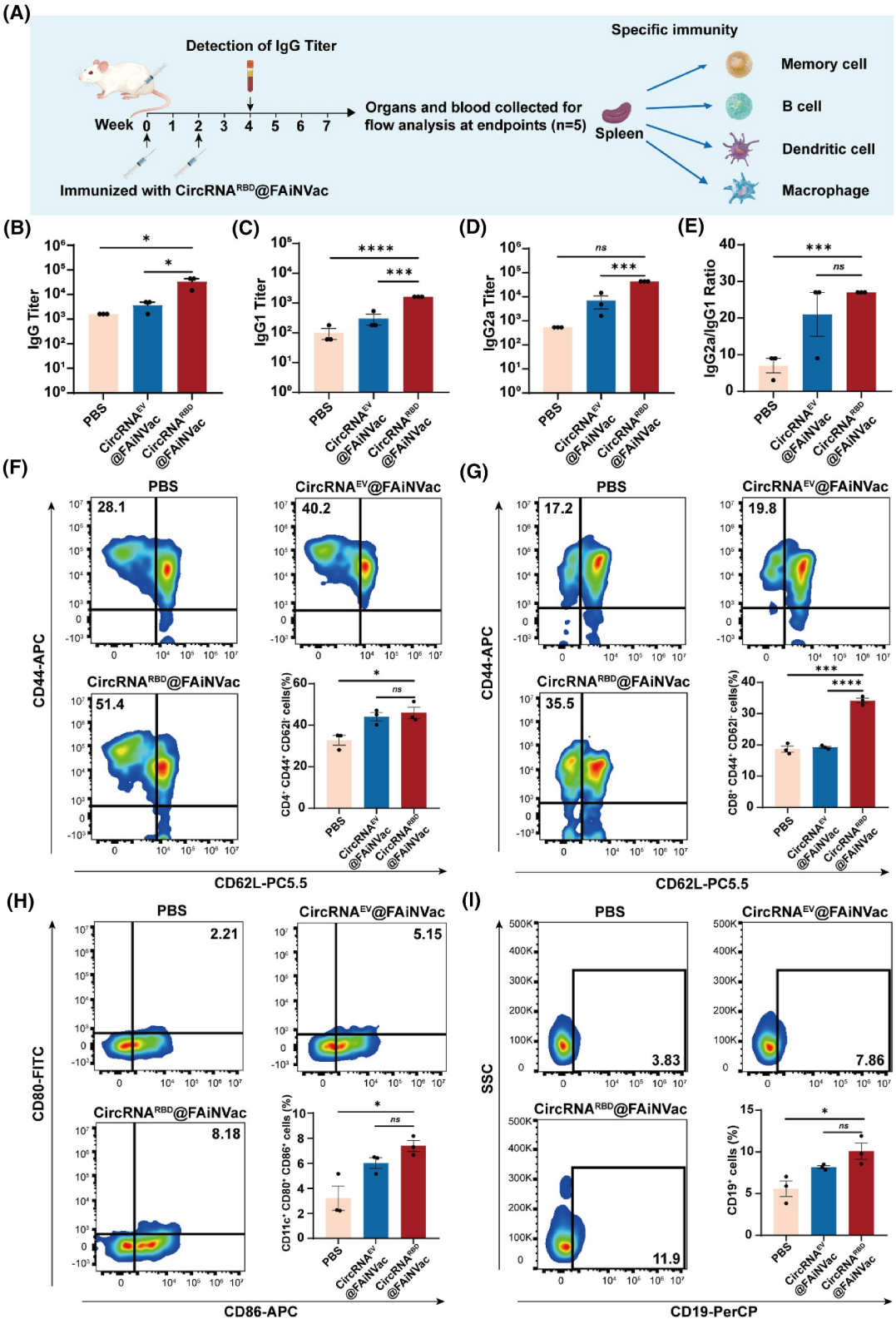

FIGURE 5 Legend on next page.

Notably, B cells, $CD4^+$ T cells, and $CD8^+$ T cells jointly mediate anti-SARS-CoV-2 immunity in patients with COVID-19. To compare the immune responses of $CD4^+$ and $CD8^+$ T cells, samples were collected from the spleen cells of immunized mice, and the effector memory T cells ($CD44^+CD62L^-$) were quantified through cellular staining (Figure 5F,G). Vaccine activity in vivo was corroborated by the enhanced activation of APCs. In mice vaccinated with

CircRNA^{RBD}@FAiNVac, the production of mature DCs and M1-type macrophages was increased compared to the control group (Figure 5H and Figure S19), indicating that the vaccine delivered the antigen to the APC in the body and activated specific immunity. Importantly, the number of B cells in mice vaccinated with CircRNA^{RBD}@FAiNVac was increased compared with the control group (Figure 5I), suggesting that the vaccine activated humoral immunity. Additionally, the immunosuppressive cells in the immunized mice decreased, and the IL-4 response produced by CD4$^+$ T_{em} cells was less (Figures S20 and S21). Notably, CircRNA^{EV}@FAiNVac (empty vector) induced moderate increases in Treg cells and IL-4 production, whereas CircRNA^{RBD}@FAiNVac (antigen-loaded) showed levels comparable to PBS (Figures S20 and S21). This differential response indicates that the empty carrier elicits a self-limiting immunoregulatory response, which is overridden in the presence of the RBD antigen. This antigen-dependent immune focusing ensures that the vaccine drives a potent, specific effector response while maintaining an inherent safety buffer against non-specific inflammation. These results indicate that the CircRNA@FAiNVac vaccine induces a Th1-biased immune response, which is consistent with a favorable immune polarization that supports effective antiviral defense without excessive Th2-associated pathology. Although systematic in vivo expression kinetics and whole-body biodistribution were not fully characterized in the present proof-of-concept study, the potent and durable humoral and cellular immune responses elicited by CircRNA^{RBD}@FAiNVac strongly support the establishment of functional and sustained antigen expression in vivo. Consistent with the intrinsic stability of circular RNA and the slow-release property of the MgPPi-based mineralized vector, CircRNA^{RBD}@FAiNVac enabled persistent antigen production within local tissues, thereby driving continuous immune activation rather than transient stimulation.

2.5 | Biosafety evaluation of CircRNA@FAiNVac nanovaccine

To comprehensively assess the safety profile of the CircRNA@FAiNVac nanovaccine, we conducted a series of in vivo toxicity studies in BALB/c mice following the vaccination protocol. Body weight monitoring over 2 weeks post-immunization revealed no significant changes, indicating an absence of acute systemic toxicity (Figure S23). To assess the in vivo biodistribution and potential off-target effects, we analyzed CircRNA@FAiNVac in different tissues after intramuscular injection. In vivo fluorescence imaging showed that over 95% of CircRNA@FAiNVac remained at the injection site, and very little spread to the systemic organs (Figure S17). Three weeks after intravenous vaccination in mice, blood was collected from the mice for hematological and biochemical analyses. As shown in Figure 6A, the inflammation-related indicators, such as white blood cells, lymphocytes (Lym), medium-sized cells (MID), and granulocytes (Neu), showed no difference compared to the PBS or CircRNA^{EV}@FAiNVac groups. Liver and kidney function indicators, including blood urea nitrogen, creatinine (CREA), alanine (ALT), and aspartate aminotransferase (AST), also remained within normal ranges, confirming no detectable organ toxicity (Figure 6B). Additionally, non-inflammatory blood indicators, including red blood cells (RBCs), hemoglobin (HGB), hematocrit (HCT), mean RBC volume (MCV), mean RBC hemoglobin (MCH), mean RBC hemoglobin concentration (MCHC), platelet volume (PCT), and platelets (PLT), all fell within the normal reference range (Figure 6C). H&E staining further confirmed the potential damage to major organs (such as heart, liver, spleen, lung, and kidney). The results indicated that the CircRNA@FAiNVac group was consistent with the PBS or CircRNA^{EV}@FAiNVac groups, and no obvious organ damage was observed (Figure 6D). Furthermore, we evaluated the long-term in vivo safety of CircRNA^{RBD}@-

FIGURE 5 CircRNA^{RBD}@FAiNVac nanovaccine elicits robust RBD-specific antibodies and immune responses. (A) Schematic diagram of vaccination and immunity of the CircRNA^{RBD}@FAiNVac nanovaccine in BALB/c mice. (B) Comparative analysis of the endpoint geometric mean titer (GMT) of SARS-CoV-2 RBD-specific IgG. (C) Comparative analysis of the endpoint GMT of SARS-CoV-2 RBD-specific IgG1. (D) Comparative analysis of the endpoint GMT of SARS-CoV-2 RBD-specific IgG2a. (E) Comparative analysis of the specific IgG2a/IgG1 ratio. Flow cytometry analysis of CD4$^+$ T cell responses (F) and CD8$^+$ T cell responses (G) after PBS, CircRNA^{EV}@FAiNVac, and CircRNA^{RBD}@FAiNVac vaccinated into mouse. (H) Flow cytometry analysis of CD80 and CD86 after PBS, CircRNA^{EV}@FAiNVac, and CircRNA^{RBD}@FAiNVac vaccinated into mouse. (I) Flow cytometry analysis of CD19 after PBS, CircRNA^{EV}@FAiNVac, and CircRNA^{RBD}@FAiNVac vaccinated into mouse. The data are shown as SEM ± mean ($n = 3$). Unpaired two-sided Student *t*-tests were conducted for comparison, as shown in the figure, *$p < 0.05$; **$p < 0.01$; ***$p < 0.001$; ****$p < 0.0001$; ns, not significant. Each symbol represents a separate mouse.

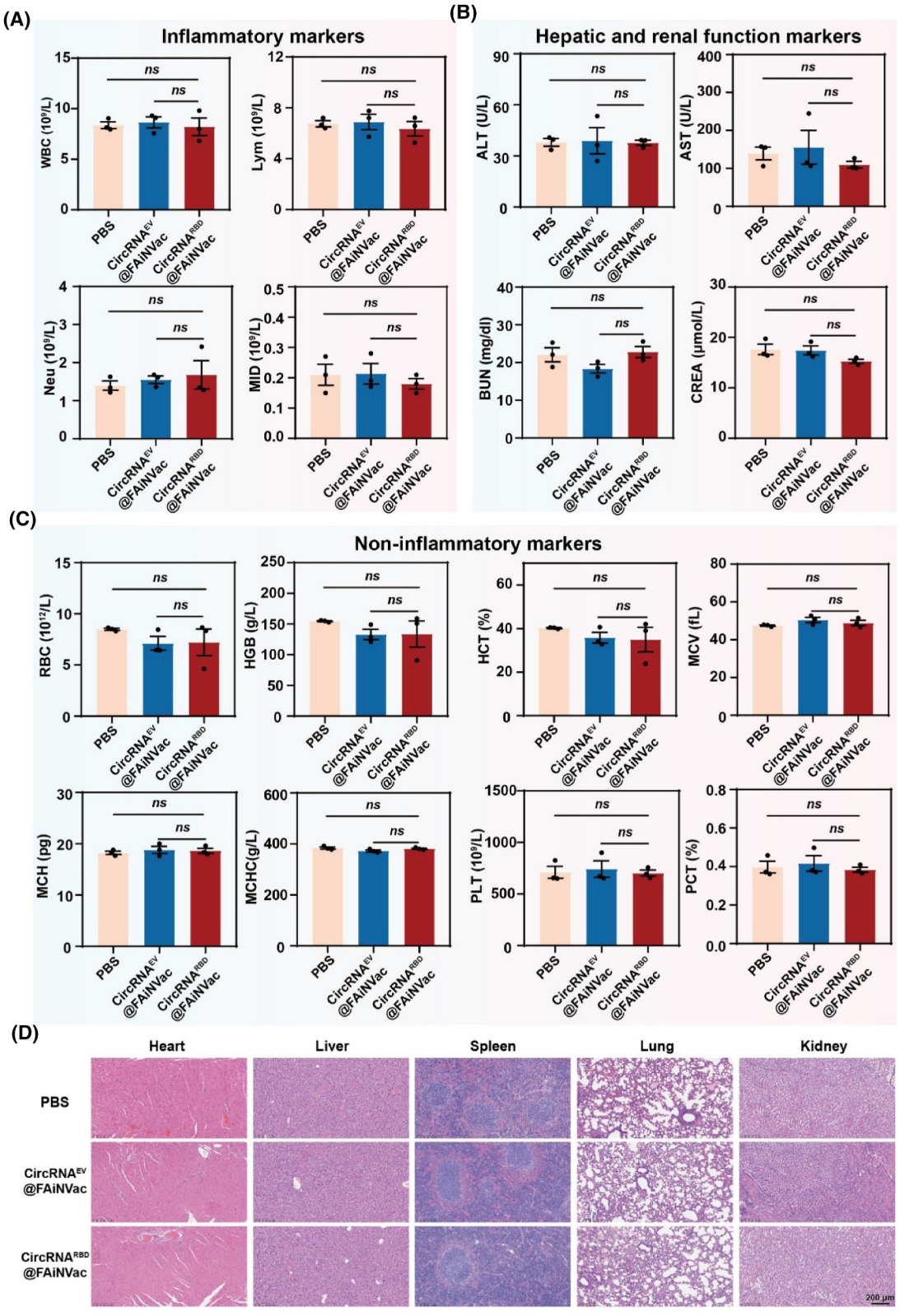

FIGURE 6 Biological safety assessment of BALB/c mice following intramuscular immunization with the CircRNA^{RBD}@FAiNVac nanovaccine. Blood biochemical analysis related to inflammatory markers (A), liver and renal function markers (B), and non-inflammatory markers (C), 3 weeks after vaccination. (D) H&E examination of the heart, liver, spleen, lungs, and kidneys. The data are shown as SEM ± mean ($n = 3$). Unpaired two-sided Student *t*-tests were conducted for comparison, as shown in the figure, *$p < 0.05$; **$p < 0.01$; ***$p < 0.001$; ****$p < 0.0001$; ns, not significant. Each symbol represents a separate mouse.

FAiNVac. Three months after vaccination, comprehensive analyses were performed, including complete blood count, liver and kidney function tests, and histopathological examination (H&E staining) of major organs. All parameters remained within normal ranges, and no obvious adverse effects or pathological abnormalities were observed, demonstrating the favorable long-term biosafety of CircRNA^{RBD}@FAiNVac (Figures S24–S27). The robust CD8+ T-cell response induced by CircRNA@FAiNVac may raise the question of potential CTL-mediated tissue damage. However, our biodistribution data mitigate this concern by demonstrating minimal off-target antigen expression in vital organs. The localized CTL activity at the injection site represents a transient, physiological clearance process that is critical for adaptive immunity but does not result in systemic toxicity, as confirmed by sensitive serum biomarkers and histopathology. The favorable biocompatibility and safety profile observed in vivo further support the unique in vivo behavior of CircRNA@FAiNVac. Unlike conventional LNP formulations that rely on synthetic lipid components and may trigger systemic inflammation or off-target accumulation in vital organs, our biomimetic mineralized vaccine is composed exclusively of biogenic ions and RNA. This innate composition contributes to its benign biological response, as evidenced by unaltered body weight, normal serum biochemical markers, and no obvious histopathological lesions in major organs. The absence of systemic toxicity and local tissue damage implies that CircRNA@FAiNVac exhibits favorable biosafety and tissue tolerance in vivo, consistent with its mild, gradually degradable, and locally oriented expression pattern. Such biocompatible in vivo behavior reduces potential adverse reactions while maintaining effective local antigen presentation, highlighting the clinical translational potential of this biomineralized RNA vaccine platform.

3 | CONCLUSION

The emergence of CircRNA@FAiNVac represents a paradigm shift in nucleic acid vaccine delivery, addressing critical limitations of conventional LNP platforms. By leveraging biomimetic mineralization principles, this study achieved the one-pot synthesis of a formulation-adjuvant integrated nanovaccine, where MgPPi nanoparticles encapsulate circRNA during RCT. Unlike LNPs, which rely on synthetic excipients with potential toxicity, CircRNA@FAiNVac consists solely of nucleic acid precursors and physiological ions, ensuring superior biocompatibility and mitigating adverse effects. This inorganic carrier not only protects circRNA from degradation but also functions as a promising adjuvant activating innate immune pathways and enhancing both humoral and cellular responses in animal studies. The sustained expression of the SARS-CoV-2 RBD antigen further demonstrates the platform's potential for durable immunization. Collectively, CircRNA@FAiNVac offers a safer, more effective, and scalable alternative to traditional delivery systems, paving the way for rapid response to emerging pathogens.

AUTHOR CONTRIBUTIONS

Liangru Lin, Yingying Ren and Jing Li contributed to data acquisition and interpretation, performed all statistical analyses, drafted and critically revised the manuscript; Jing Li, Panxing Ren, Xinran Wang, Yixin Ding, and Linsu Liu contributed to data acquisition and analysis; Cong Liu, Zhou Li, Yan Liu and Dan Luo contributed to conception, design, data acquisition and interpretation, drafted and critically revised the manuscript. All authors gave their final approval and agree to be accountable for all aspects of the work.

ACKNOWLEDGEMENTS

The authors are grateful for the support received from the National Natural Science Foundation of China (52372174, 82230030, T2125003), National Key Research and Development Program of China (2022YFB3205602), Beijing Nova Programme Interdisciplinary Cooperation Project (No. 20250484970).

CONFLICT OF INTEREST STATEMENT

The authors declare no conflicts of interest.

DATA AVAILABILITY STATEMENT

The data that support the findings of this study are available from the corresponding author upon reasonable request.

ETHICS STATEMENT

Female BALB/c mice and C57BL/6 mice, aged 6–8 weeks, were purchased from SPF (Beijing) Biotechnology Co., Ltd. All mice were bred and housed under specific pathogen-free (SPF) conditions. All animal experiments were approved by the Animal Ethics Committee of Beijing Institute of Nanoenergy and Nanosystems, Chinese Academy of Sciences (Approval Number: 2024012LD). All experimental operations were performed in strict accordance with the *Guide for the Care and Use of Laboratory Animals* issued by the National Institutes of Health (NIH).

ORCID

Liangru Lin https://orcid.org/0009-0000-0744-3849
Zhou Li https://orcid.org/0000-0002-9952-7296
Yan Liu https://orcid.org/0000-0002-8193-6729
Dan Luo https://orcid.org/0000-0002-4657-6131

REFERENCES

1. W. Chen, K. R. Tompkins, I. W. Windsor, L. T. Martinez, M. Ramos, W. Li, S. Shrivastava, S. Rajput, J. S. Chang, P. Sahasrabudhe, K. F. Fennell, T. J. McLellan, G. M. West, K. P. Dizon, A. Yam, S. Mitra, S. Saha, D. Sharaf, A. P. McKeen, C. I. Cadima, A. Muik, W. Swanson, R. Munoz Moreno, P. Mendoza Daroca, U. Sahin, A. S. Anderson, H. Wu, K. A. Swanson, K. Modjarrad, *Nat. Commun.* **2025**, *16*, 10914.
2. C. M. Miller, J. K. Moen, A. Iwasaki, *Trends Immunol.* **2025**, *47*, 9.
3. S. Huang, K. M. Cohen, L. Chen, X. Kang, C. Liu, M. E. Demouth, W. Jiang, A. R. Maldeney, R. Tong, Z. Ke, K. Chandran, W. Luo, Q. Yin, *Adv. Sci.* **2026**, *13*, e12100.
4. J. Scott, M. S. Abers, H. K. Marwah, N. C. McCann, E. A. Meyerowitz, A. Richterman, D. F. Fleming, E. J. Holmes, L. E. Moat, S. G. Redepenning, E. A. Smith, C. J. Stoddart, M. E. Sundaram, A. K. Ulrich, C. Alba, C. J. Anderson, M. K. Arpey, E. Borre, J. Ladines-Lim, A. J. Mehr, K. Rich, C. Watts, N. E. Basta, J. Jarolimova, R. P. Walensky, C. M. Dugdale, *N. Engl. J. Med.* **2025**, *393*, 2221.
5. L. Lin, Y. Pei, Z. Li, D. Luo, *Interdiscip. Med.* **2023**, *1*, e20220008.
6. T. Li, T. Zhang, Y. Gu, S. Li, N. Xia, *Fundam. Res.* **2021**, *1*, 139.
7. D. Fitz-Patrick, D. S. McVinnie, L. A. Jackson, G. Crowther, A. Geevarughese, K. D. Cannon, L. M. Garcia, Puebla Y. Pineiro, Z. Yi, L. Cunliffe, A. Maniar, A. M. Zareba, C. A. Ianos, E. Gomme, K. Koury, P. Suphaphiphat Allen, A. S. Anderson, A. Gurtman, K. Lindert, *N. Engl. J. Med.* **2025**, *393*, 2001.
8. S. J. Jung, J. J. Seo, S. Lee, S. I. Hyun, J. E. Lee, S. Lee, Y. Lee, H. Chang, H. Lee, J. H. Kim, V. N. Kim, *Nat. Biotechnol.* **2025**, https://doi.org/10.1038/s41587-025-02891-7.
9. H. Zhang, H. Liu, Y. Xu, H. Huang, Y. Liu, J. Wang, Y. Qin, H. Wang, L. Ma, Z. Xun, X. Hou, T. K. Lu, J. Cao, *Science* **2025**, *390*, eadr8470.
10. L. J. Kubiatowicz, A. Mohapatra, N. Krishnan, R. H. Fang, L. Zhang, *Exploration* **2022**, *2*, 20210217.
11. Y. Zhang, X. Zhang, Y. Gao, S. Liu, *BMEMat* **2025**, *3*, e12116.
12. L. Qu, Z. Yi, Y. Shen, L. Lin, F. Chen, Y. Xu, Z. Wu, H. Tang, X. Zhang, F. Tian, C. Wang, X. Xiao, X. Dong, L. Guo, S. Lu, C. Yang, C. Tang, Y. Yang, W. Yu, J. Wang, Y. Zhou, Q. Huang, A. Yisimayi, S. Liu, W. Huang, Y. Cao, Y. Wang, Z. Zhou, X. Peng, J. Wang, X. S. Xie, W. Wei, *Cell* **2022**, *185*, 1728.
13. D. Niu, Y. Wu, J. Lian, *Signal Transduct. Target. Ther.* **2023**, *8*, 341.
14. K. C. Liao, M. Eshaghi, Z. Hong, T. Y. Saw, J. A. J. Lim, J. Han, J. G. A. Aw, K. Y. Tan, A. Yap, X. Gao, Y. A. Cheng, S. Y. Lim, Y. Z. N. Cheang, W. A. A. Saron, A. P. S. Rathore, L. Zhang, B. Shunmuganathan, R. Gupta, S. L. I. Tan, X. Qian, K. Purushotorman, N. Subramaniam, L. A. Vardy, P. A. Macary, A. John, Y. Y. Yang, S. Alonso, H. Song, R. G. Huber, Y. Wan, *Nucleic Acids Res.* **2025**, *53*, gkaf089.
15. Y. Wang, L. Lin, X. Wang, J. Li, Q. Pan, H. Kou, J. Yin, F. Gao, X. Liao, C. Zhang, Q. Yin, C. Zhao, X. Li, J. Lin, Y. Xu, M. Qiu, D. Luo, L. Qu, *Cell Rep. Med.* **2025**, *6*, 102250.
16. S. Chen, C. Wu, D. Wang, J. Zhuang, Z. Li, B. Li, W. Pan, B. Liu, *Adv. Mater.* **2026**, *38*, e18041.
17. Y. Xiao, B. Wu, Q. Zhou, F. Wu, N. Li, C. Xu, X. Han, *Trends Mol. Med.* **2025**, *31*, 1047.
18. Y. Chen, E. De Lombaerde, A. Bugler-Lamb, Z. Zhong, M. J. Schuijs, C. M. B. Gomez, J. De Baere, M. Gontsarik, H. Lauwers, K. Deswarte, N. N. Sanders, B. N. Lambrecht, M. Guilliams, B. G. De Geest, *Angew. Chem. Int. Ed.* **2025**, *64*, e202506954.
19. D. O. Lopez-Cantu, X. Wang, H. Carrasco-Magallanes, S. Afewerki, X. Zhang, J. V. Bonventre, G. U. Ruiz-Esparza, *Nano-Micro Lett.* **2022**, *14*, 41.
20. D. Pei, *ACS Nano* **2025**, *19*, 40293.
21. Q. Yin, C. Zhang, J. Li, K. Huang, M. Qiu, *Adv. Sci.* **2026**, *13*, e12535.
22. Z. Belhadj, Y. Qie, R. P. Carney, Y. Li, G. Nie, *BMEMat* **2023**, *1*, e12018.
23. T. Kovačič, H. Haas, L. Stotsky-Oterin, A. Štrancar, U. Bren, D. Peer, *Nat. Rev. Chem* **2025**, *9*, 790.
24. M. Vadovics, W. Zhao, E. F. Daley, K. Lam, O. Daly, K. Rashid, H. R. Lee, P. Schreiner, K. A. Lundgreen, B. T. Gaudette, V. V. Shuvaev, E. Arguiri, H. Muramatsu, A. Sárközy, T. Mdluli, J. Xu, X. Han, N. De Luna, D. Castaño, E. Bettini, E. Ábrahám, Z. Lipinszki, G. Carlucci, A. H. Bansode, K. Nguyen, T. M. Le, T. Luu, V. R. Muzykantov, P. Bates, D. Allman, M. J. Mitchell, M. Locci, C. G. Radu, J. Heyes, N. Pardi, *Nat. Nanotechnol.* **2025**, *20*, 1312.
25. P. I. Back, M. Yu, S. Modaresahmadi, S. Hajimirzaei, Q. Zhang, M. R. Islam, A. A. Schwendeman, N. M. La-Beck, *ACS Nano* **2024**, *18*, 28480.
26. S. K. Patel, M. M. Billingsley, C. Frazee, X. Han, K. L. Swingle, J. Qin, M.-G. Alameh, K. Wang, D. Weissman, M. J. Mitchell, *J. Control. Release* **2022**, *347*, 521.
27. M. Z. C. Hatit, C. N. Dobrowolski, M. P. Lokugamage, D. Loughrey, H. Ni, C. Zurla, A. J. Da Silva Sanchez, A. Radmand, S. G. Huayamares, R. Zenhausern, K. Paunovska, H. E. Peck, J. Kim, M. Sato, J. I. Feldman, M.-A. Rivera, A. Cristian, Y. Kim, P. J. Santangelo, J. E. Dahlman, *Nat. Chem.* **2023**, *15*, 508.
28. S. Omo-Lamai, Y. Wang, M. N. Patel, A. Milosavljevic, D. Zuschlag, S. Poddar, J. Wu, L. Wang, F. Dong, C. Espy, A. Majumder, E.-O. Essien, M. Shen, B. Channer, T. E. Papp, M. Tobin, R. Maheshwari, S. Jeong, S. Patel, A. Shah, S. Murali, L. S. Chase, M. E. Zamora, M. L. Arral, O. A. Marcos-Contreras, J. W. Myerson, C. A. Hunter, D. Discher, P. J. Gaskill, A. Tsourkas, V. R. Muzykantov, I. Brodsky, S. Shin, K. A. Whitehead, H. Parhiz, J. Katzen, J. J. Miner, D. Trauner, J. S. Brenner, *Nat. Nanotechnol.* **2025**, *20*, 1285.
29. J. You, S. Liu, J. Liang, Q. Feng, M. Duan, Z. Ali, L. Chen, Z. Wang, *MedMat* **2024**, *1*, 104.
30. Y. Hu, Y. Chen, H. Tang, G. Zhang, M. Ma, Z. Pan, Q. Bai, W. Lin, R. Cao, L. Wang, B. Xu, L. Wang, L. Zhang, Y. Gu, M. Yang, Y. She, W. Sun, C. Chen, *MedMat* **2025**, *2*, 33.
31. E. Zhu, Y.-R. Li, Z. Liu, S. Wang, *MedMat* **2024**, *1*, 51.
32. J. Wang, J. Hou, H. Lu, S. Bai, Y. Chen, W. Yang, S. Wang, G. Li, Y. Wei, X. Wang, W. Xie, *MedMat* **2025**, *2*, 1.

33. J. Ji, L. Li, W. Guo, J. Zhang, Y. Yao, H. Chen, F. Liao, Z. Jin, L. Liu, J. Ouyang, X.-J. Liang, *Fundam. Res.* **2025**, *5*, 1889.
34. D. Sun, W. Tan, J. Zhao, Y. Tian, S. Li, Z. Zhang, X. Dong, X. Liu, N. Liu, P. Jiao, J. Ma, *Fundam. Res.* **2025**, *5*, 2948.
35. T. Kim, H. S. Han, K. Yang, Y. M. Kim, K. Nam, K. H. Park, S. Y. Choi, H. W. Park, K. Y. Choi, Y. H. Roh, *ACS Nano* **2024**, *18*, 7972.
36. D. T. Thoresen, D. Galls, B. Götte, W. Wang, A. M. Pyle, *Mol. Cell* **2023**, *83*, 90.
37. F. G. Bauernfeind, G. Horvath, A. Stutz, E. S. Alnemri, K. MacDonald, D. Speert, T. Fernandes-Alnemri, J. Wu, B. G. Monks, K. A. Fitzgerald, V. Hornung, E. Latz, *J. Immunol.* **2009**, *183*, 787.
38. K. V. Swanson, M. Deng, J. P. Ting, *Nat. Rev. Immunol.* **2019**, *19*, 477.
39. C. Li, M. Chen, X. He, D. Ouyang, *Acta Biochim. Biophys. Sin.* **2021**, *53*, 131.
40. B. Hussain, Y. Xie, U. Jabeen, D. Lu, B. Yang, C. Wu, G. Shang, *Front. Immunol.* **2022**, *13*, 808607.
41. T. Abe, G. N. Barber, *J. Virol.* **2014**, *88*, 5328.
42. Z. Hu, X. Yu, R. Ding, B. Liu, C. Gu, X. W. Pan, Q. Han, Y. Zhang, J. Wan, X. G. Cui, J. Sun, Q. Zou, *J. Clin. Investig.* **2023**, *133*, e166031.
43. J. Wang, S. Wang, T. Ye, F. Li, X. Gao, Y. Wang, P. Ye, S. Qing, C. Wang, H. Yue, J. Wu, W. Wei, G. Ma, *Adv. Sci.* **2020**, *7*, 2001108.
44. Q. Lu, H. Yang, Y. Peng, Z. Dong, P. Nie, G. Wang, S. Luo, X. Min, J. Huang, M. Huang, *Front. Immunol.* **2024**, *15*, 1473193.

SUPPORTING INFORMATION

Additional supporting information can be found online in the Supporting Information section at the end of this article.

How to cite this article: L. Lin, Y. Ren, J. Li, P. Ren, X. Wang, Y. Ding, L. Liu, C. Liu, Z. Li, Y. Liu, D. Luo, *Interdiscip. Med*. **2026**, e70135. https://doi.org/10.1002/inmd.70135